Pacific North American circulation pattern links external forcing and North American hydroclimatic change over the past millennium

Zhongfang Liu[a,1], Yanlin Tang[b], Zhimin Jian[a], Christopher J. Poulsen[c], Jeffrey M. Welker[d], and Gabriel J. Bowen[e,f,1]

[a]State Key Laboratory of Marine Geology, Tongji University, Shanghai 200092, China; [b]School of Mathematical Sciences, Tongji University, Shanghai 200092, China; [c]Department of Earth and Environmental Sciences, University of Michigan, Ann Arbor, MI 48109; [d]Department of Biological Sciences, University of Alaska Anchorage, Anchorage, AK 99508; [e]Department of Geology and Geophysics, University of Utah, Salt Lake City, UT 84112; and [f]Global Change and Sustainability Center, University of Utah, Salt Lake City, UT 84112

Edited by Mark H. Thiemens, University of California, San Diego, La Jolla, CA, and approved February 14, 2017 (received for review November 2, 2016)

Land and sea surface temperatures, precipitation, and storm tracks in North America and the North Pacific are controlled to a large degree by atmospheric variability associated with the Pacific North American (PNA) pattern. The modern instrumental record indicates a trend toward a positive PNA phase in recent decades, which has led to accelerated warming and snowpack decline in northwestern North America. The brevity of the instrumental record, however, limits our understanding of long-term PNA variability and its directional or cyclic patterns. Here we develop a 937-y-long reconstruction of the winter PNA based on a network of annually resolved tree-ring proxy records across North America. The reconstruction is consistent with previous regional records in suggesting that the recent persistent positive PNA pattern is unprecedented over the past millennium, but documents patterns of decadal-scale variability that contrast with previous reconstructions. Our reconstruction shows that PNA has been strongly and consistently correlated with sea surface temperature variation, solar irradiance, and volcanic forcing over the period of record, and played a significant role in translating these forcings into decadal-to-multidecadal hydroclimate variability over North America. Climate model ensembles show limited power to predict multidecadal variation in PNA over the period of our record, raising questions about their potential to project future hydroclimatic change modulated by this circulation pattern.

paleoclimate | atmospheric circulation | Holocene | climate change | North America

Recent drought intensification (1, 2) and mountain snowpack declines (3, 4) have raised concerns about future water shortages and wildfires throughout western North America, from the southwestern United States to Alaska (5, 6). Although many lines of evidence have pointed to the impact of anthropogenic warming (3, 7, 8), naturally occurring atmospheric variability also contributes to the observed changes (9–11). It has been suggested that changes in upper tropospheric circulation associated with the Pacific North American (PNA) pattern (12), in particular, have played a large role in shaping recent variation in North American hydroclimate (11, 13–15). For example, changes in cool-season PNA account for 30 to 50% of the variance in 1 April snow water equivalent or precipitation in the Pacific Northwest (14–16). A positive PNA pattern is associated with greater meridional flow due to enhancement of a ridge over the Rocky Mountains and a trough over the southeastern United States. This mode leads to warming in northwestern North America and cooling in the southeastern United States (Fig. 1*A*), drier conditions in the Pacific Northwest and northern central California, and wetter conditions in the southwestern United States and western Great Plains (Fig. 1*B*). In contrast, the negative PNA pattern corresponds to more zonal flow, with weather anomalies opposite those associated with positive PNA.

Although PNA is recognized as a dominant control on intra-annual and interannual hydroclimate variability in North America (17) and may contribute to multidecadal variability via interactions with other climate teleconnections and forcings (18, 19), instrumental records of the PNA are available only since 1948 (12) and are insufficient to document long-term PNA behavior, its drivers, and interactions. Longer reconstructions of PNA variability have been developed from paleoproxy records and historical climate data. Tree-ring-based reconstructions (hereafter PNA_{Trouet}) (19) and ice core records (20) from western North America suggest a secular trend toward the positive PNA phase since the 1850s, overlain by periodic oscillations, but cover only the past three centuries. A millennium-long reconstruction (hereafter PNA_{Hubeny}) from lake sediment records (Fig. 1) in the northeast United States has also been argued to reflect hemispheric patterns of circulation attributable to PNA variation (21). Although these reconstructions show reasonably good agreement within the calibration periods, they often share little resemblance before the instrumental era. For example, the PNA_{Trouet} and PNA_{Hubeny} indices only share 1.9% of their variance for the period 1725–1949. Disagreement between these indices may reflect regional biases of the proxy data assembled in each study and/or nonstationarity of the relationship between local climate and large-scale circulation, casting doubt on the capacity for data from a single PNA-sensitive region to accurately record long-term changes in this large-scale circulation mode (22, 23).

To address these shortcomings, we develop a reconstruction of the PNA variability for the past millennium by combining multiple

Significance

We have developed a new reconstruction of changes in the wintertime atmospheric circulation over North America based on data distributed across the region. The record spans almost 1,000 years and shows how variation in ocean temperatures, solar energy, volcanic eruptions, and greenhouse gases has affected circulation over this period. We show that the circulation pattern is strongly correlated with fluctuating drought conditions in the western United States. Climate models do a poor job of simulating the reconstructed record of circulation change, and thus may have difficulty predicting future patterns of drought influenced by changing winter storm tracks across this region.

Author contributions: Z.L. and G.J.B. designed research; Z.L., C.J.P., and G.J.B. performed research; Z.L. and Y.T. analyzed data; and Z.L., Z.J., C.J.P., J.M.W., and G.J.B. wrote the paper.

The authors declare no conflict of interest.

This article is a PNAS Direct Submission.

[1]To whom correspondence may be addressed. Email: gabe.bowen@utah.edu or liuzf406@gmail.com.

This article contains supporting information online at www.pnas.org/lookup/suppl/doi:10.1073/pnas.1618201114/-/DCSupplemental.

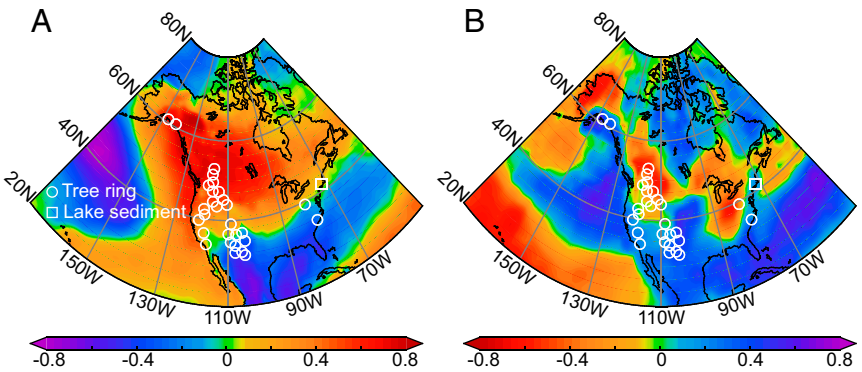

Fig. 1. Map of North America showing the location of 29 tree-ring proxy records used in this study. The background color shows the correlations of the instrumental PNA with (*A*) temperature from the European Centre for Medium-Range Weather Forecasts (ECMWF) Interim Reanalysis (ERA-Interim) (68) and (*B*) Global Precipitation Climatology Project precipitation (69) during the winter (December through March) for the period 1980–2015. All of the records cover at least the period 1062–1998 (see *SI Appendix*, Table S1). Some symbols have been slightly displaced to make them visible on the map. The composite sedimentary record used in PNA_{Hubeny} is also shown.

tree-ring proxy records from different PNA-sensitive regions (24). Our reconstruction (PNA_{Liu}) provides a robust, long-term baseline for the interpretation of PNA data from the instrumental era and documents the evolution of PNA and its environmental impacts in the preinstrumental era. In addition, our time series supports comparison with other historical and proxy-based climate system records, improving our understanding of links between PNA atmospheric variability and external forcing such as Pacific sea surface temperatures (SSTs) [El Niño/Southern Oscillation (ENSO); Pacific Decadal Oscillation (PDO)] (25), solar activity, and strong volcanic eruptions.

Proxy Selection and Reconstruction

We present a millennium-long reconstruction of winter (December through March, the season when the PNA is most strongly expressed) PNA variability from an array of 29 annually resolved tree-ring records and ring-based proxy reconstructions that represent winter PNA fingerprints in temperature and precipitation across North America (Fig. 1 and *SI Appendix*, Table S1). Multimodel (26) (see *SI Appendix*, Table S2) ensemble reconstructions suggest that the spatial structure of climate variability associated with PNA is largely stable over the past millennium (see *SI Appendix*, Figs. S1 and S2), supporting the use of spatially proxy networks to reconstruct the long-term history of the PNA. We restricted our analysis to those records that encompass the medieval period, are precisely dated, and are significantly ($P < 0.1$) correlated with instrumental winter PNA index (*Methods*). Most of these records have been used previously for reconstructions of interannual to multidecadal snowpack (3, 15) and drought variability (1, 27) over North America with a high level of fidelity.

Our reconstruction was developed using a well-tested principal component regression (PCR) procedure (28). Common components of variability among the records were extracted using a principal components analysis (PCA) and then retained to build a linear regression model by calibrating on the instrumental winter PNA index over a period of overlap between proxy and instrumental records (*Methods*). The reconstruction explains 55% ($P < 0.0001$, $T = 7.46$, $n_{eff} = 48$) of the winter PNA variance over the instrumental period (Fig. 2*A*) and shows good statistical skill (*Methods*; see *SI Appendix*, Table S2).

PNA Variability and Teleconnections

The reconstructed history of winter PNA over the period 1062–1998 is presented in Fig. 2*B*, along with the instrumental PNA record. Our reconstruction is significantly ($P < 0.01$) correlated with existing proxy-based PNA records and with PNA indices derived from reanalysis and historical data over the common intervals (see *SI Appendix*, Table S4), confirming that the reconstruction closely tracks the upper tropospheric atmospheric signature of the PNA (Fig. 2 *C* and *D*). In contrast to the two previous long-term reconstructions (PNA_{Trouet} and PNA_{Hubeny}) (19, 21), our reconstruction incorporates proxies from both western and eastern North America and exhibits a much-improved explained variance for instrumental and historical PNA records (see *SI Appendix*, Table S4).

Our reconstruction shows significant PNA variation on interannual to interdecadal timescales throughout the period of record (Fig. 2*B*). Spectral (29) and wavelet (30) analyses reveal dominant quasi-periodicities at around 2 to 3, ~19, and ~74 y (see *SI Appendix*, Fig. S3*A*). Interannual (~3 y) variability, which is strongly expressed throughout the instrumental period (31), persists throughout the past millennium. The 74-y cycle is also a dominant periodicity and is present during most of past millennium (see *SI Appendix*, Fig. S3*B*). Among the most prominent features our reconstruction shares with previous records (19–21) is a secular trend

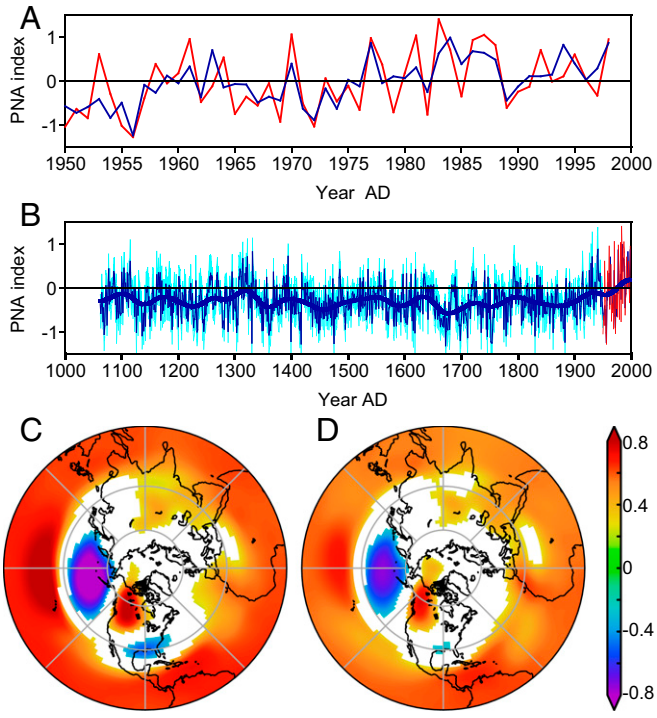

Fig. 2. (*A*) Instrumental (red line) and reconstructed (blue line) winter PNA indices for the calibration period 1950–1998. (*B*) Winter PNA reconstruction (thin blue line; 1062–1998 values standardized relative to the calibration period) along with instrumental PNA index (red line). The cyan shading around the reconstruction shows two-sided 95% bootstrap confidence intervals (see *SI Appendix*), and the thick blue line represents a 70-y cubic smoothing spline. (*C* and *D*) Spatial correlations of the winter 500-hPa geopotential height field (70) with (*C*) instrumental and (*D*) reconstructed PNA indices during the period 1950–1998. Only areas with significance at the $P < 0.05$ level are shown in color.

toward a positive PNA phase since the 1850s, which is punctuated by a decade-long PNA minimum centered on the 1950s followed by a rapid rise in the late 20th century. Our reconstruction clearly shows that the extreme positive state of the PNA pattern characterizing the late 20th century (1980–1998) is unprecedented during the past 1,000 y (see *SI Appendix*). Before the 1850s, multidecadal periods of extreme negative PNA phase were centered on 1140, 1230, 1350, 1450, 1580, 1670, and 1750.

PNA_{Liu} is significantly correlated with a 500-y reconstruction of cool-season 500-hPa geopotential height fields (32) over the Pacific and North America sectors (PNA_{Wise}; $r = 0.36$, $P < 0.0001$, $T = 8.08$, $n_{eff} = 440$). In the low-frequency domain, both indices show many common peaks and troughs, with pronounced minima around 1670, 1750, and 1860 (Fig. 3*A*). Our reconstruction shows less similarity with PNA_{Hubeny} at interannual timescales ($r = 0.13$, $P < 0.001$, $T = 3.14$, $n_{eff} = 577$). Both records show some centennial-scale intervals dominated by positive or negative anomalies, but PNA_{Liu} exhibits less low-frequency variability than PNA_{Hubeny}, and there is little concurrence in these patterns among the two records (Fig. 3*B*). Multidecadal periods centered on *ca*. 1120, 1170, 1360, 1400, 1500, 1640, and 1700 are characterized by substantial, opposite-signed shifts in PNA phase as reconstructed by the two methods. Another prominent contrast between the records is the stronger expression of intermediate-frequency signals (such as the ∼19- and ∼74-y variability) in PNA_{Liu} (Fig. 3*B*). Although these differences may arise from a number of sources, bias and/or noise resulting from additional non-PNA influences (e.g., increased dating uncertainty back in time for composite sedimentary records (33, 34) and local climate) on regional proxy records are a likely contributor. These biases should be minimized by the use of a spatially distributed network of records in PNA_{Liu} (see *SI Appendix*, Table S4).

We compare PNA_{Liu} with proxy-based reconstructions of SST modes that affect North American climate today. PNA_{Liu} shows some broad similarity to a PDO index reconstruction (35), although the two records are not significantly correlated ($r = 0.18$, $P > 0.1$, $T = 0.75$, $n_{eff} = 19$ for 11-y moving averages; Fig. 3*C*), and is significantly correlated with reconstructed Niño 3.4 index values (36) ($r = 0.41$, $P < 0.05$, $T = 2.58$, $n_{eff} = 35$ for 11-y moving averages; Fig. 3*D*). The nature and relative strength of these correlations resemble relationships observed between instrumental PNA and PDO/ENSO records, suggesting that modulation of the PNA phases by Pacific SSTs, observed in the instrumental era, is probably a persistent feature over the past millennium.

The dominance of positive PNA anomalies since *ca.* 1800 is linked to an enhanced Aleutian Low (AL) over the North Pacific (see *SI Appendix*, Fig. S4), leading to intensified meridional circulation over North America. The strongest multidecadal periods of negative PNA_{Liu} anomaly occur in the late 17th to mid-18th centuries, coinciding with a weaker AL during the height of the Little Ice Age (LIA) (*SI Appendix*, Fig. S4). This suggests that peak LIA cooling was characterized by a more zonal circulation over North America (37), in contrast with earlier suggestions that the LIA was a period of more meridional circulation (38). The strong negative PNA pattern during the LIA may be associated with strong negative PDO or La Niña conditions (Fig. 3 *C* and *D*) and may have contributed to anomalously high snowpack (3) and glacial advance (39) in the northern Rocky Mountain region. Previous studies have suggested the occurrence of a persistent positive North Atlantic Oscillation (NAO) state (40) or negative PDO (35) during the Medieval Climate Anomaly (MCA). We find no evidence of such a state in the PNA and ENSO reconstructions (Fig. 3).

Interannual to interdecadal variability in PNA_{Liu} is also well matched with fluctuations in Palmer Drought Severity Index (PDSI) reconstructions (1) from the western United States ($r = 0.33$, $P < 0.001$, $T = 9.65$, $n_{eff} = 764$ for annual averages and $r = 0.43$, $P < 0.01$, $T = 3.05$, $n_{eff} = 43$ for 11-y moving averages; Fig. 3*E*). Our full reconstruction shares some records in common with the millennial PDSI reconstructions, which may artificially strengthen this correlation, but a rarified reconstruction retaining only records

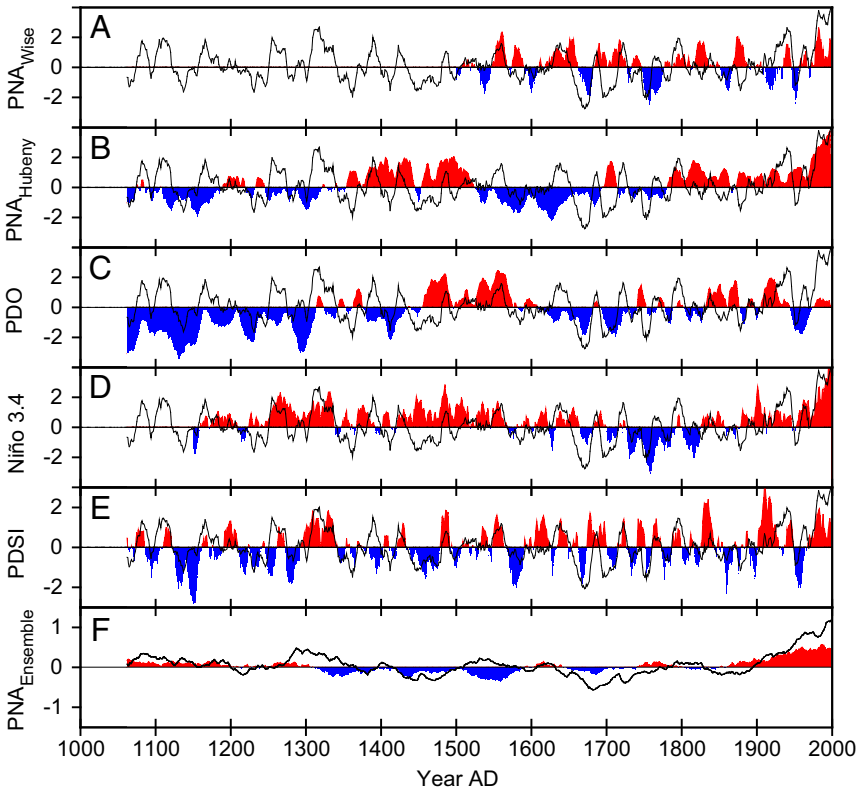

Fig. 3. Comparison of our PNA reconstruction with other proxy reconstructions and climate model simulations. Our reconstruction (black line) along with (*A*) PNA_{Wise} derived from reconstructed cool-season 500-hPa geopotential heights (32), (*B*) PNA_{Hubeny} (21), (*C*) PDO index (35), (*D*) Niño 3.4 index (36), (*E*) area-averaged PDSI (1) for the western USA (25°N to 45°N and 120°W to 95°W; see *SI Appendix*, Fig. S7), and (*F*) ensemble mean PNA index across seven CMIP5 simulations. All records are shown as 11-y moving averages relative to the period 1500–1980 except for the PNA reconstruction–simulation comparison (70-y moving averages) shown in *F*.

not included in the PDSI work independently confirms the PNA–PDSI correlation (see *SI Appendix*, Table S1 and Fig. S5). Major historical droughts including the Medieval Drought (1) (around 1150), the Dust Bowl of the 1930s, and the severe 1950s drought in the western and southwestern United States are coincident with low PNA_{Liu} anomalies (see *SI Appendix*, Fig. S6).

In addition to its direct impact on winter storm tracks and snowpack, the positive wintertime PNA pattern is normally associated with a northward displacement of the subsequent summer anticyclone over western North America, leading to wet summer conditions in the southwestern United States (41) (see *SI Appendix*, Fig. S7). Reconstructed North American hydroclimate variability over the past millennium features a leading spatial mode similar to the modern PNA/PDSI pattern, with widespread droughts centered on the American southwest and opposite conditions in the Pacific Northwest (11, 15, 27) (see *SI Appendix*, Fig. S7). Together with the strong PNA/PDSI time series correlation demonstrated by our record, this similarity in spatial pattern reconstruction supports a strong linkage between PNA-associated circulation changes and western North American hydroclimate throughout the past millennium (21).

Although SST variability (e.g., ENSO and PDO) has long been recognized as a main driver of western North American drought (1, 42), our PNA reconstruction explains slightly more multidecadal variance (19%) in the PDSI record than do ENSO (13%, $P < 0.05$, $T = 2.59$, $n_{eff} = 47$) or PDO (12%, $P < 0.05$, $T = 2.05$, $n_{eff} = 32$) reconstructions. This strong correlation between PNAA and PDSI appears to agree with recent simulations that highlight the role of atmospheric circulation variability in driving western North American droughts (9, 10). The positive trend of winter PNA in recent decades has led to warmer temperatures in northwestern North America (43, 44) due to enhanced southwesterly flows (45) and compressional heating (46), resulting in more winter precipitation falling as rain instead of snow and in earlier spring snow melt. These effects, in conjunction with accelerated warming, have led to unusual snowpack declines (3, 14, 15), drought (6), wildfire (47, 48), and even changes in forest phenology (46) across parts of western North America.

Comparison with Model Simulations

To determine the extent to which climate models independently replicate the observed fluctuations in PNA pattern over the past millennium, we calculate PNA indices from seven CMIP5 model simulations (see *SI Appendix*). The simulated winter PNA indices for individual models share little similarity with each other and with PNA_{Liu} (see *SI Appendix*, Fig. S8). In the low-frequency domain, the model ensemble shares some similarity, but is not significantly correlated, with our PNA index reconstruction ($r = 0.63$, $P > 0.1$, $T = 1.41$, $n_{eff} = 5$ for 70-y moving averages; Fig. 3*F*). Both the models and proxy reconstruction suggest positive PNA anomalies since the late 1800s, with increasing strength toward the present. Periods of strong negative PNA anomaly during the LIA are common to the model and proxy reconstructions, although the timing of these periods within the LIA is not consistent. A previously recognized discrepancy between modeled and reconstructed PNA in the early nineteenth century (24) is strongly expressed in the comparison with PNA_{Liu}. The general lack of agreement between the proxies and models may suggest that this small ensemble of models is not accurately capturing last millennium internal variability as expressed by the PNA pattern.

External Forcing of PNA Variability

PNA variability is driven by both internal atmospheric dynamics and external forcings. Observational studies suggest that ENSO variability in the equatorial Pacific can produce Rossby wave propagation from the tropical Pacific to the extratropics, directly exciting a PNA-like pattern with a positive (negative) phase during El Niño (La Niña) (49). The 2- to 3-y periodicity identified in our PNA reconstruction falls within the conventional modern ENSO band (2 y to 7 y), which, together with significant correlation ($r = 0.28$, $P < 0.001$, $T = 7.93$, $n_{eff} = 741$) between reconstructed PNA and Niño 3.4 indices, suggests that ENSO may be a source of interannual PNA variability over the past millennium.

The observed PNA variability on interdecadal timescales may similarly be forced by PDO, which has modern frequencies of 15 y to 25 y and 50 y to 70 y (25), or by a low-frequency component of ENSO (19). Given these PNA teleconnections, periods of strong La Niña- and negative PDO-like SST anomalies during the LIA could have contributed to a negative PNA pattern during this interval. In contrast, the persistent positive PNA anomaly since the late 1800s may be due partly to strengthening of El Niño (36) (Fig. 3*D*). The establishment of unprecedented positive winter PNA index in the late 20th century also closely parallels the human-induced rise in greenhouse gas (GHG)

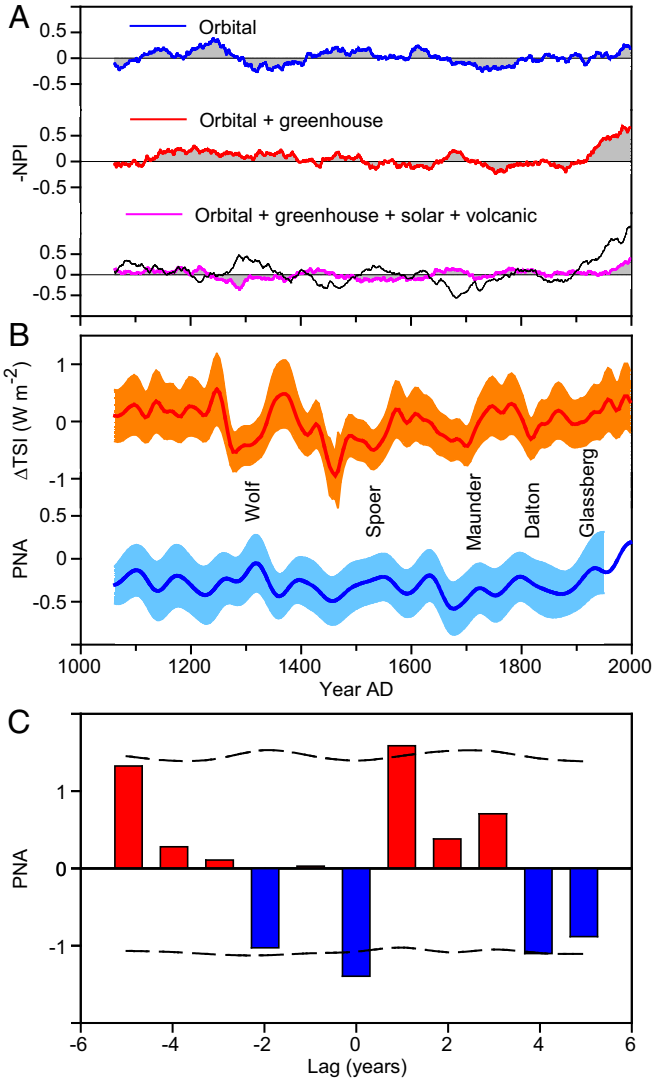

Fig. 4. PNA response to external forcings. (*A*) Modeled NPI (–PNA) variability for different radiative forcings in CSIRO Mk3L (52) and reconstructed PNA index (PNA_{Liu}; black line). All are shown as 70-y moving averages. (*B*) Total solar irradiance anomaly (54) (ΔTSI; red line) and PNA index (blue). Well-known solar minima are labeled. The PNA is smoothed using 70-y spline. Orange and blue shading indicate 1 SE and 95% confidence level, respectively. (*C*) Composite PNA response to the 14 strongest volcanic eruptions (see *SI Appendix*, Table S5). The average over different volcanic eruptions is shown at a range of lag times, e.g., with lag 1 indicating the first winter after the eruption. Dashed lines show the 10 to 90% confidence intervals derived from 1,000 Monte Carlo simulations (*Methods*).

concentrations, implying that human activity may be forcing the increasingly positive state of the PNA pattern (50, 51). This theory is supported by a set of last-millennium model experiments (52) (*Methods*), in which greenhouse forcing causes a deepened AL (measured by the North Pacific Index (12), NPI; Fig. 4*A*), akin to the condition during the positive phase of PNA.

Changes in radiative forcings such as solar irradiance and strong volcanic eruptions are also important drivers of climate variability over the last millennium (53). Analysis of circulation changes and non-GHG radiative forcing over the last millennium may provide some support for linking these forcings to PNA variation. However, the above-referenced last-millennium model experiments show little improvement in fit to PNA_{Liu} when solar irradiance and volcanic forcings are added to orbital and greenhouse influences (Fig. 4*A*). The PNA reconstruction itself demonstrates a weak (not significant, $P > 0.1$) antiphased relationship with reconstructed total solar irradiance anomalies (54) (ΔTSI; Fig. 4*B*). Short-term solar minima (maxima) typically correspond to maxima (minima) in PNA_{Liu}, supporting a similar association previously observed in observations (55) and the three-century PNA_{Trouet} reconstruction (19). The influence of volcanic forcing on PNA is more strongly supported in the PNA_{Liu} record. A superposed epoch analysis (56) of PNA_{Liu} response to the strongest 14 volcanic eruptions (see *SI Appendix*, Table S5) during the past millennium shows that positive PNA anomalies are consistently observed during the first posteruption winter ($P < 0.1$; Fig. 4*C*). A similar relationship was previously documented for a small number of eruptions during the 20th century (57, 58).

Together, these results suggest a strong and consistent relationship between changing radiative forcing and Northern Hemisphere midlatitude circulation over the past millennium. The dynamics underlying this relationship remain debated but may involve stratospheric–tropospheric dynamics or related cloud feedbacks (59, 60) that amplify small solar and volcanic signals and influence the position and strength of the AL and the PNA pattern. PNA circulation changes thus provide a mechanism linking multiple radiative forcings to structured, spatially heterogeneous variation in climate and drought across North America during the period of our analysis and, potentially, in the future.

Conclusions

Our reconstruction of a winter PNA index from a distributed network of proxy records documents PNA variability and dynamics during the past millennium. Results indicate that, on interannual and interdecadal timescales, the PNA interacts with Pacific SST, solar, volcanic, and GHG forcings to modulate North American hydroclimate variability. The recent positive PNA pattern is unprecedented over the past millennium, likely aggravating snowpack decline (14, 15), drought (6), and wildfire (48, 61) across parts of the northwestern United States and moderating drought conditions in the southwestern United States (21). The PNA reconstruction not only provides a framework for understanding North American hydroclimate variability but also provides a benchmark for evaluating model simulations of the PNA (24), raising questions about the ability of current models to accurately predict future hydroclimate change in the region.

Methods

Proxy Record Selection and Processing. Proxy records of North American hydroclimate (temperature, precipitation, drought, moisture balance, and stream flow) were obtained from public repositories (e.g., International Tree-Ring Data Bank https://www.ncdc.noaa.gov/data-access/paleoclimatology-data/datasets/tree-ring) or by direct request from the authors. The 29 tree-ring proxy records used in this study meet three criteria: They (*i*) provide continuous records supported by at least five replicate ring-width measurements spanning the period 1062–1998, (*ii*) are precisely dated and have annual resolution, and (*iii*) are significantly ($P < 0.1$) correlated with the instrumental PNA index (Fig. 1; see *SI Appendix*, Table S1).

The records were not subjected to additional postprocessing and reflect the original data provided by the authors. Although the use of different processing and detrending methods may influence the preservation of low-frequency signal in the individual records, we defer to specialist decisions on the appropriateness of processing methods for each record. Variation in processing likely adds some random noise to the composite reconstruction, but any imparted bias should be minimized by the large number of records used.

PNA Reconstruction. The reconstruction was developed using a (28) PCR procedure similar to that previously used in NAO reconstruction (62). Individual records were standardized over the period 1062–1998 and used to build a time–space data matrix. A PCA was performed on the standardized records to create a set of orthogonal principal components (PCs). There is no universally agreed upon procedure for selection of the optimal number of PCs to retain. We used the Kaiser–Guttman rule (63) and scree graphs (64) to select the first 10 PCs, which cumulatively explain 90% of the variance in the dataset. We regressed the instrumental PNA index on these PCs and retained components that were significantly correlated with the index for the final model. These were the first, second, third, seventh, and eighth PCs, with the first, second, and seventh PCs significant at $P < 0.05$ and the third and eighth PCs significant at $P < 0.10$ and $P = 0.28$, respectively.

Validation Tests. The model was trained over the full (1950–1998) 49-y interval of overlap between the instrumental PNA index and tree-ring proxy records. Considering the relatively short duration of the instrumental record, we did not adopt the widely used split calibration/validation scheme (28). Instead, we validated our reconstruction against three sets of independent, preinstrumental PNA records. First, we compared our reconstruction with PNA index values calculated from the Twentieth Century Reanalysis version 2 (20CRv2) (65) and the European Centre for Medium-Range Weather Forecasts (ECMWF) Reanalysis (ERA) Twentieth Century reanalysis (ERA-20C) (66) for the period 1901–1949. Second, two expressions (NPI_{Obs} and NPI_{Jones}; see *SI Appendix*, Table S3) of the winter North Pacific index (NPI, a surrogate for the PNA index, see below) based on instrumental climate records were used to validate our reconstruction for the periods 1900–1949 and 1873–1949, respectively. Third, a reconstructed PNA index (67) based on historical station data, which has been well validated, was compared with our reconstruction for the period 1922–1949. Reconstruction validity was assessed using Pearson's correlation coefficient, reduction of error (RE) and coefficient of efficiency (CE) statistics (see *SI Appendix*, Table S3), which strongly support the validity of the reconstruction.

Radiative Forcing and PNA Response. To evaluate the response of the PNA to different radiative forcing mechanisms, the output from a set of sensitivity experiments using the Commonwealth Scientific and Industrial Research Organization (CSIRO) Mk3L (52) was analyzed. The model experiments include last-millennium simulations run with the cumulative addition of orbital, GHG, solar and volcanic forcings (three ensemble members each; ftp://ftp.ncdc.noaa.gov/pub/data/paleo/gcmoutput/phipps2014/). Because only surface climate fields are available, we use monthly resolution mean sea level pressure fields to calculate the North Pacific Index (NPI), which is defined as the area-weighted sea level pressure over the region 30°N to 65°N, 160°E to 140°W (12). The NPI serves as a surrogate for the PNA index, as evidenced by the correlation of −0.90 between the winter mean NPI and PNA indices for the period of 1950–1998 (see *SI Appendix*, Table S4).

Superposed Epoch Analysis. We performed a superposed epoch analysis (56) to determine the response of the PNA to each strong volcanic eruption over the past millennium (see *SI Appendix*, Table S5). We took the years of eruptions as "key dates." We then sampled the reconstructed PNA index time series using an 11-y window centered on the key date (i.e., five data points on either side of the key date). The extracted windows were stacked to form an "eruption matrix." The statistical significance of the average PNA response to the eruptions was determined using a Monte Carlo approach, in which the analysis was repeated 1,000 times using randomly selected years for key dates. We compared reconstructed PNA index values for each year in the eruption matrix with the 10 to 90% percentile levels of the Monte Carlo distribution.

ACKNOWLEDGMENTS. We thank Xiaogang He for his help with tree-ring data collection and Haimao Lan for assistance with model data processing. We also thank Bradford Hubeny and Tracy Ewen for providing access to reconstructed PNA data. We acknowledge the International Tree-Ring Data Bank and the CMIP5/PMIP3 communities for making available proxy data and model outputs. This work was supported by the China Young 1000-Talent Program and National Natural Science Foundation of China Grant 41171022 (to Z.L.) and National Science Foundation Award EF-1241286 (to G.J.B.).

1. Cook ER, Woodhouse CA, Eakin CM, Meko DM, Stahle DW (2004) Long-term aridity changes in the western United States. *Science* 306(5698):1015–1018.
2. Woodhouse CA, Meko DM, MacDonald GM, Stahle DW, Cook ER (2010) A 1,200-year perspective of 21st century drought in southwestern North America. *Proc Natl Acad Sci USA* 107(50):21283–21288.
3. Pederson GT, et al. (2011) The unusual nature of recent snowpack declines in the North American cordillera. *Science* 333(6040):332–335.
4. Belmecheri S, Babst F, Wahl ER, Stahle DW, Trouet V (2016) Multi-century evaluation of Sierra Nevada snowpack. *Nat Clim Change* 6(1):2–3.
5. Csank AZ, Miller AE, Sherriff RL, Berg EE, Welker JM (2016) Tree-ring isotopes reveal drought sensitivity in trees killed by spruce beetle outbreaks in south-central Alaska. *Ecol Appl* 26(7):2001–2020.
6. Sauchyn DJ, St-Jacques JM, Luckman BH (2015) Long-term reliability of the Athabasca River (Alberta, Canada) as the water source for oil sands mining. *Proc Natl Acad Sci USA* 112(41):12621–12626.
7. Williams AP, et al. (2015) Contribution of anthropogenic warming to California drought during 2012–2014. *Geophys Res Lett* 42(16):6819–6828.
8. Diffenbaugh NS, Swain DL, Touma D (2015) Anthropogenic warming has increased drought risk in California. *Proc Natl Acad Sci USA* 112(13):3931–3936.
9. Coats S, Cook BI, Smerdon JE, Seager R (2015) North American pancontinental droughts in model simulations of the Last Millennium. *J Clim* 28(5):2025–2043.
10. Stevenson S, Timmermann A, Chikamoto Y, Langford S, DiNezio P (2015) Stochastically generated North American megadroughts. *J Clim* 28(5):1865–1880.
11. Wise EK (2016) Five centuries of US West Coast drought: Occurrence, spatial distribution, and associated atmospheric circulation patterns. *Geophys Res Lett* 43(9): 4539–4546.
12. Wallace JM, Gutzler DS (1981) Teleconnections in the geopotential height field during the Northern Hemisphere winter. *Mon Weather Rev* 109(4):784–812.
13. Balling RC, Goodrich GB (2010) Increasing drought in the American Southwest? A continental perspective using a spatial analytical evaluation of recent trends. *Phys Geogr* 31(4):293–306.
14. Abatzoglou JT (2011) Influence of the PNA on declining mountain snowpack in the Western United States. *Int J Climatol* 31(8):1135–1142.
15. Pederson GT, Betancourt JL, McCabe GJ (2013) Regional patterns and proximal causes of the recent snowpack decline in the Rocky Mountains, US. *Geophys Res Lett* 40(9): 1811–1816.
16. Mote PW (2006) Climate-driven variability and trends in mountain snowpack in Western North America. *J Clim* 19(23):6209–6220.
17. Leathers DJ, Yarnal B, Palecki MA (1991) The Pacific/North American teleconnection pattern and United States climate. Part I: Regional temperature and precipitation associations. *J Clim* 4(5):517–528.
18. Trenberth KE, Hurrell JW (1994) Decadal atmosphere-ocean variations in the Pacific. *Clim Dyn* 9(6):303–319.
19. Trouet V, Taylor AH (2010) Multi-century variability in the Pacific North American circulation pattern reconstructed from tree rings. *Clim Dyn* 35(6):953–963.
20. Moore GW, Holdsworth G, Alverson K (2002) Climate change in the North Pacific region over the past three centuries. *Nature* 420(6914):401–403.
21. Hubeny JB, King JW, Reddin M (2011) Northeast US precipitation variability and North American climate teleconnections interpreted from late Holocene varved sediments. *Proc Natl Acad Sci USA* 108(44):17895–17900.
22. Lehner F, Raible CC, Stocker TF (2012) Testing the robustness of a precipitation proxy-based North Atlantic Oscillation reconstruction. *Quat Sci Rev* 45:85–94.
23. Raible CC, Lehner F, González-Rouco JF, Fernández-Donado L (2014) Changing correlation structures of the Northern Hemisphere atmospheric circulation from 1000 to 2100 AD. *Clim Past* 10:537–550.
24. Zanchettin D, et al. (2015) Reconciling reconstructed and simulated features of the winter Pacific/North American pattern in the early 19th century. *Clim Past* 11(6): 939–958.
25. Mantua NJ, Hare SR (2002) The Pacific decadal oscillation. *J Oceanogr* 58(1):35–44.
26. Taylor KE, Stouffer RJ, Meehl GA (2012) An overview of CMIP5 and the experiment design. *Bull Am Meteorol Soc* 93(4):485–498.
27. Herweijer C, Seager R, Cook ER, Emile-Geay J (2007) North American droughts of the last millennium from a gridded network of tree-ring data. *J Clim* 20(7):1353–1376.
28. Cook ER, D'Arrigo RD, Mann ME (2002) A well-verified, multiproxy reconstruction of the winter North Atlantic Oscillation Index since ad 1400. *J Clim* 15(13):1754–1764.
29. Schulz M, Mudelsee M (2002) REDFIT: Estimating red-noise spectra directly from unevenly spaced paleoclimatic time series. *Comput Geosci* 28(3):421–426.
30. Torrence C, Compo GP (1998) A practical guide to wavelet analysis. *Bull Am Meteorol Soc* 79(1):61–78.
31. Yu B, Tang Y, Zhang X, Niitsoo A (2009) An analysis on observed and simulated PNA associated atmospheric diabatic heating. *Clim Dyn* 33(1):75–91.
32. Wise EK, Dannenberg MP (2014) Persistence of pressure patterns over North America and the North Pacific since AD 1500. *Nat Commun* 5:4912.
33. Hubeny JB, King JW, Cantwell M (2009) Anthropogenic influences on estuarine sedimentation and ecology: Examples from the varved sediments of the Pettaquamscutt River Estuary, Rhode Island. *J Paleolimnol* 41(2):297–314.
34. Hilfinger MF, IV, Mullins HT, Burnett A, Kirby ME (2001) A 2500 year sediment record from Fayetteville Green Lake, New York: Evidence for anthropogenic impacts and historic isotope shift. *J Paleolimnol* 26(3):293–305.
35. MacDonald GM, Case RA (2005) Variations in the Pacific Decadal Oscillation over the past millennium. *Geophys Res Lett* 32(8):L08703.
36. Emile-Geay J, Cobb KM, Mann ME, Wittenberg AT (2013) Estimating central equatorial Pacific SST variability over the past millennium. Part II: Reconstructions and implications. *J Clim* 26(7):2329–2352.
37. Anderson L, Abbott MB, Finney BP, Burns SJ (2005) Regional atmospheric circulation change in the North Pacific during the Holocene inferred from lacustrine carbonate oxygen isotopes, Yukon Territory, Canada. *Quat Res* 64(1):21–35.
38. Crowley TJ, North GR (1991) *Paleoclimatology* (Oxford Univ Press, New York).
39. Luckman BH (2000) The little ice age in the Canadian Rockies. *Geomorphology* 32(3): 357–384.
40. Trouet V, et al. (2009) Persistent positive North Atlantic Oscillation mode dominated the medieval climate anomaly. *Science* 324(5923):78–80.
41. Carleton AM, Carpenter DA, Weser PJ (1990) Mechanisms of interannual variability of the southwest United States summer rainfall maximum. *J Clim* 3(9):999–1015.
42. Cook ER, Seager R, Cane MA, Stahle DW (2007) North American drought: Reconstructions, causes, and consequences. *Earth Sci Rev* 81(1):93–134.
43. Johnstone JA, Mantua NJ (2014) Atmospheric controls on northeast Pacific temperature variability and change, 1900–2012. *Proc Natl Acad Sci USA* 111(40):14360–14365.
44. Liu Z, et al. (2015) Recent contrasting winter temperature changes over North America linked to enhanced positive Pacific North American pattern. *Geophys Res Lett* 42(18):7750–7757.
45. Luce CH, Abatzoglou JT, Holden ZA (2013) The missing mountain water: Slower westerlies decrease orographic enhancement in the Pacific Northwest USA. *Science* 342(6164):1360–1364.
46. Ault TR, Macalady AK, Pederson GT, Betancourt JL, Schwartz MD (2011) Northern Hemisphere modes of variability and the timing of spring in western North America. *J Clim* 24(15):4003–4014.
47. Westerling AL, Hidalgo HG, Cayan DR, Swetnam TW (2006) Warming and earlier spring increase western US forest wildfire activity. *Science* 313(5789):940–943.
48. Trouet V, Taylor AH, Carleton AM, Skinner CN (2006) Fire-climate interactions in forests of the American Pacific coast. *Geophys Res Lett* 33(18):L18704.
49. Horel JD, Wallace JM (1981) Planetary-scale atmospheric phenomena associated with the Southern Oscillation. *Mon Weather Rev* 109(4):813–829.
50. Brandefelt J, Körnich H (2008) Northern Hemisphere stationary waves in future climate projections. *J Clim* 21(23):6341–6353.
51. Moore JC, et al. (2014) Arctic sea ice and atmospheric circulation under the GeoMIP G1 scenario. *J Geophys Res* 119(2):567–583.
52. Phipps SJ, et al. (2013) Paleoclimate data-model comparison and the role of climate forcings over the past 1500 years. *J Clim* 26(18):6915–6936.
53. Jones PD, Mann ME (2004) Climate over past millennia. *Rev Geophys* 42(2):RG2002.
54. Steinhilber F, Beer J, Fröhlich C (2009) Total solar irradiance during the Holocene. *Geophys Res Lett* 36(19):L19704.
55. Liu Z, Yoshimura K, Buenning NH, He X (2014) Solar cycle modulation of the Pacific–North American teleconnection influence on North American winter climate. *Environ Res Lett* 9(2):024004.
56. Brad Adams J, Mann ME, Ammann CM (2003) Proxy evidence for an El Niño-like response to volcanic forcing. *Nature* 426(6964):274–278.
57. Christiansen B (2008) Volcanic eruptions, large-scale modes in the Northern Hemisphere, and the El Niño-Southern Oscillation. *J Clim* 21(5):910–922.
58. Liu Z, Yoshimura K, Buenning NH, Jian Z, Zhao L (2016) The response of winter Pacific North American pattern to strong volcanic eruptions. *Clim Dyn*, 10.1007/s00382-016-3287-0.
59. Van Loon H, Meehl GA, Shea DJ (2007) Coupled air-sea response to solar forcing in the Pacific region during northern winter. *J Geophys Res* 112(D2):D02108.
60. Stenchikov G, et al. (2002) Arctic Oscillation response to the 1991 Mount Pinatubo eruption: Effects of volcanic aerosols and ozone depletion. *J Geophys Res* 107(D24): 4803.
61. Gedalof Z, Peterson DL, Mantua NJ (2005) Atmospheric, climatic, and ecological controls on extreme wildfire years in the northwestern United States. *Ecol Appl* 15(1): 154–174.
62. Ortega P, et al. (2015) A model-tested North Atlantic Oscillation reconstruction for the past millennium. *Nature* 523(7558):71–74.
63. Jackson JE (2005) *A User's Guide to Principal Components* (Wiley, New York).
64. Wilks DS (2011) *Statistical Methods in the Atmospheric Sciences* (Academic, New York).
65. Compo GP, et al. (2011) The Twentieth Century Reanalysis Project. *Q J R Meteorol Soc* 137(654):1–28.
66. Poli P, et al. (2013) *The Data Assimilation System and Initial Performance Evaluation of the ECMWF Pilot Reanalysis of the 20th-Century Assimilating Surface Observations Only (ERA-20C)* (Eur Cent Medium-Range Weather Forecast, Reading, UK), ERA Rep Ser 14.
67. Ewen T, Brönnimann S, Annis J (2008) An extended Pacific-North American Index from upper-air historical data back to 1922. *J Clim* 21(6):1295–1308.
68. Dee D, et al. (2011) The ERA-Interim reanalysis: Configuration and performance of the data assimilation system. *Q J R Meteorol Soc* 137(656):553–597.
69. Adler RF, et al. (2003) The version-2 Global Precipitation Climatology Project (GPCP) monthly precipitation analysis (1979-present). *J Hydrometeorol* 4(6):1147–1167.
70. Kalnay EC, et al. (1996) The NCEP/NCAR 40-year reanalysis project. *Bull Am Meteorol Soc* 77(3):437–471.